

High-spin states in the semimagic nucleus ^{89}Y and neutron-core excitations in the $N = 50$ isotones

Z. Q. Li (李志泉),¹ S. Y. Wang (王守宇),^{1,*} C. Y. Niu (牛晨阳),¹ B. Qi (亓斌),¹ S. Wang (王硕),¹ D. P. Sun (孙大鹏),¹ C. Liu (刘晨),¹ C. J. Xu (徐长江),¹ L. Liu (刘雷),¹ P. Zhang (张盼),¹ X. G. Wu (吴晓光),² G. S. Li (李广生),² C. Y. He (贺创业),² Y. Zheng (郑云),² C. B. Li (李聪博),² B. B. Yu (于蓓蓓),² S. P. Hu (胡世鹏),² S. H. Yao (姚顺和),² X. P. Cao (曹雪鹏),² and J. L. Wang (汪金龙)²

¹Shandong Provincial Key Laboratory of Optical Astronomy and Solar-Terrestrial Environment, Institute of Space Sciences,

Shandong University, Weihai 264209, China

²China Institute of Atomic Energy, Beijing 102413, China

(Received 31 January 2016; published 19 July 2016)

The semimagic nucleus ^{89}Y has been investigated using the $^{82}\text{Se}(^{11}\text{B},4n)$ reaction at beam energies of 48 and 52 MeV. More than 24 new transitions have been identified, leading to a considerable extension of the level structures of ^{89}Y . The experimental results are compared with the large-basis shell model calculations. They show that cross-shell neutron excitations play a pivotal role in high-spin level structures of ^{89}Y . The systematic features of neutron-core excitations in the $N = 50$ isotones are also discussed.

DOI: [10.1103/PhysRevC.94.014315](https://doi.org/10.1103/PhysRevC.94.014315)

I. INTRODUCTION

The structures of nuclei in the $A \sim 80$ mass region have attracted considerable theoretical and experimental attention in recent years because of a number of interesting nuclear phenomena predicted and also observed, such as signature inversion [1], shape coexistence [2,3], magnetic rotation [4,5], chiral doublet bands [6], and most recently multiple chiral doublet bands with octupole correlations [7]. In this mass region, the shell structure effects are quite strong. In particular to the $N = 50$ isotones, the properties of nuclei are essentially influenced by the proton subshell and shell closures at $Z = 38$, 40, and 50 due to the successive filling into the $2p_{3/2}$, $2p_{1/2}$, and $1g_{9/2}$ orbits. In the $N = 50$ isotones, the positive and negative parity states generated by the neutron-core excitations across the $N = 50$ shell closure have been reported in ^{88}Sr [8], ^{90}Zr [9], ^{91}Nb [10], ^{92}Mo [11], and ^{93}Tc [12].

The present work focuses on the semimagic nucleus ^{89}Y ($Z = 39$, $N = 50$), which is of particular interest because it lies just in between $Z = 38$ and 40 subshell closures. The previous studies [13–16] suggested that the high angular momentum positive parity states of ^{89}Y are dominated by the neutron-core excitations. However, the negative parity states corresponding to the breaking of the $N = 50$ core have not yet been reported. Thus, it is interesting to investigate high-spin states of ^{89}Y , which could not only yield a better understanding of this semimagic nucleus but also explore the systematic properties of neutron-core excitations across the $N = 50$ shell closure in $A \sim 80$ mass region.

Prior to this work, high-spin states of ^{89}Y were investigated by in-beam γ -ray spectroscopy [13,15,17–20]. Recently, an unpublished doctoral thesis [15] extended the level scheme of ^{89}Y up to an excitation energy of $E \sim 11.3$ MeV. In the present article, we report new experimental results on high-spin states of ^{89}Y using the heavy-ion fusion-evaporation reaction $^{82}\text{Se}(^{11}\text{B},4n)$. The article is organized as follows. The

experimental procedures are described in Sec. II. Section III of this article presents the experimental results and the construction of the level scheme. The experimental level energies are compared to shell model calculations within different configuration spaces in Sec. IV. The phenomenon of neutron-core excitations in the $N = 50$ isotones is discussed in Sec. V. Finally, the article is closed with conclusions in the last section.

II. EXPERIMENTAL DETAILS

High-spin states of ^{89}Y were populated using the $^{82}\text{Se}(^{11}\text{B},4n)^{89}\text{Y}$ reaction at beam energies of 48 and 52 MeV. The beam was delivered by the HI-13 tandem accelerator at the China Institute of Atomic Energy (CIAE) in Beijing. The target consisted of 1.35 mg/cm^2 of enriched ^{82}Se rolled onto a 9.1 mg/cm^2 Pb backing. The main exit channels of the reaction were produced by the evaporation of four and five neutrons leading to $^{88,89}\text{Y}$ isotopes. The experimental results of ^{88}Y by this data set have been reported in Ref. [21]. The deexcitation γ rays were detected by an array of 12 Compton-suppressed hyperpure-germanium (HPGe) detectors and two low-energy photon spectrometer (LEPS) detectors. Five HPGe detectors were placed at 90° , four at 40° or 140° , and the remainder of HPGe detectors at 30° , 50° , and 150° with respect to the beam axis. In total, about 1.3×10^8 γ - γ coincidence events were recorded. In the offline analysis, all the coincidence events were sorted into a 4096 by 4096 channel symmetrized E_γ - E_γ matrix. To determine the multipolarity of the emitted γ rays, two asymmetric angular distribution from oriented states (ADO) [22] matrices were constructed. The ADO ratio was defined as $I_\gamma(\text{at } \sim 40^\circ, 140^\circ)/I_\gamma(\text{at } \sim 90^\circ)$, where $I_\gamma(\text{at } \sim 40^\circ, 140^\circ)$ and $I_\gamma(\text{at } \sim 90^\circ)$ are the total intensities of the γ ray of interest observed in the detectors at 40° or 140° and 90° , respectively. The typical ADO ratios for stretched quadrupole or $\Delta I = 0$ dipole transitions and stretched pure dipole transitions are found to be ~ 1.1 and ~ 0.7 , respectively.

*Corresponding author: sywang@sdu.edu.cn

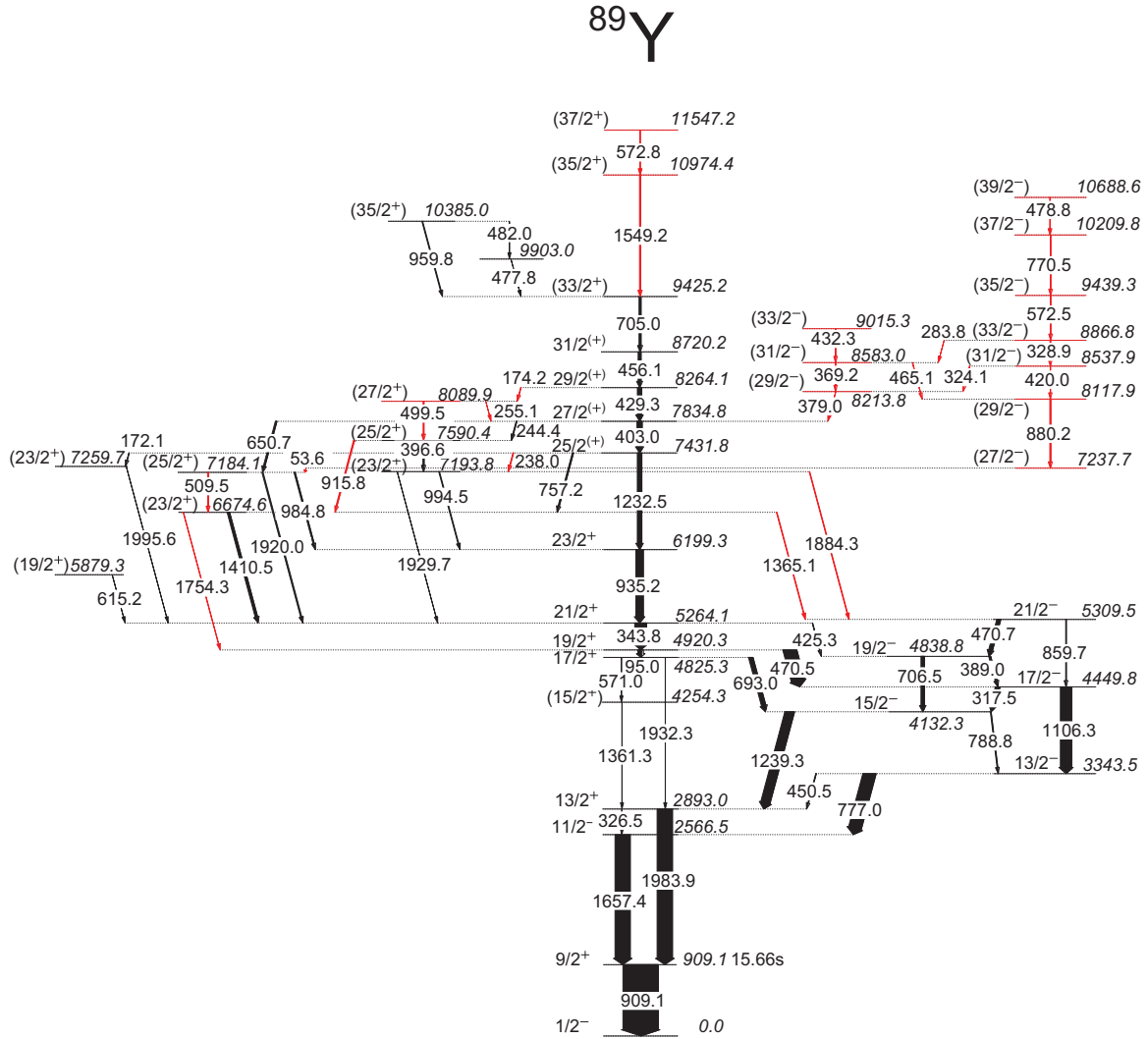


FIG. 1. Level scheme of ^{89}Y established in the present work. New transitions and levels observed in the current work are denoted in red.

III. EXPERIMENTAL RESULTS

Compared with the recent doctoral thesis [15], we added 13 new levels and 24 new transitions into the level scheme of ^{89}Y . The updated level scheme of ^{89}Y is shown in Fig. 1, and new transitions (levels) are marked in red. Typical prompt γ - γ coincidence spectra for ^{89}Y are shown in Fig. 2. The spin and parity assignments are based on the previous assignments [13,15] and the present measured ADO ratios of the γ rays. The energies and relative intensities of the observed γ rays, together with the measured ADO ratios and other relevant information concerning their placements in the level scheme, are listed in Table I. Extensions and alterations of the level scheme with respect to the previous studies are discussed in the following.

For the positive parity states, nine new transitions and three new levels are observed, extending these levels to an excitation energy of ~ 11.5 MeV. These new transitions can be seen in Figs. 2(a) and 2(b). In addition, we have changed the placement of the 915.8 keV transition. In Ref. [15], the 915.8 keV transition was placed above the 10385.0 keV level. From the

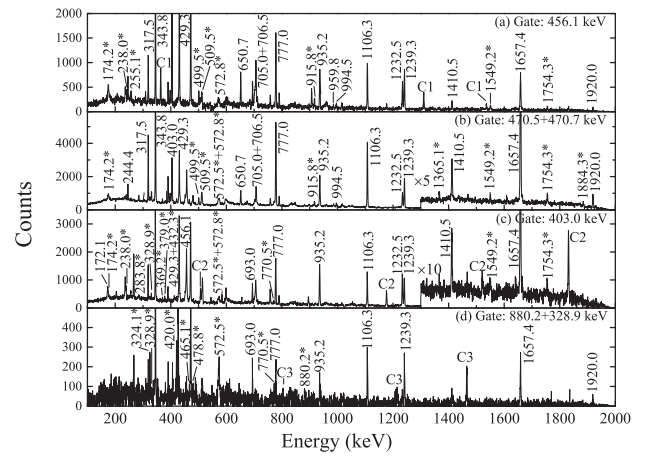


FIG. 2. Spectra of γ -rays gated on the 456.1, 470.5+470.7, 403.0, and 880.2+328.9 keV transitions, respectively. The newly observed transitions are indicated by asterisks. Peaks labeled C1, C2, and C3 in the spectra originate from the contaminations of ^{89}Sr [23], ^{87}Rb [24], and ^{84}Kr [25], respectively.

TABLE I. γ -ray energies, relative intensities, measured ADO ratios, initial and final level energies, and spin-parity assignments of the transitions in ^{89}Y .

E_γ (keV)	I_γ	R_{ADO}	$E_i \rightarrow E_f$ (keV)	$I_i^\pi \rightarrow I_f^\pi$
53.6			7237.7 → 7184.1	(27/2 ⁻) → (25/2 ⁺)
95.0	26.5(22)	0.83(23)	4920.3 → 4825.3	19/2 ⁺ → 17/2 ⁺
172.1	4.4(9)	0.78(27)	7431.8 → 7259.7	25/2 ⁽⁺⁾ → (23/2 ⁺)
174.2	4.8(9)	0.87(23)	8264.1 → 8089.9	29/2 ⁽⁺⁾ → (27/2 ⁺)
238.0	3.9(8)		7431.8 → 7193.8	25/2 ⁽⁺⁾ → (23/2 ⁺)
244.4	8.1(10)	0.81(14)	7834.8 → 7590.4	27/2 ⁽⁺⁾ → (25/2 ⁺)
255.1	4.7(9)		8089.9 → 7834.8	(27/2 ⁺) → 27/2 ⁽⁺⁾
283.8	3.8(7)		8866.8 → 8583.0	(33/2 ⁻) → (31/2 ⁻)
317.5	29.2(18)	0.85(13)	4449.8 → 4132.3	17/2 ⁻ → 15/2 ⁻
324.1	3.5(8)	0.83(36)	8537.9 → 8213.8	(31/2 ⁻) → (29/2 ⁻)
326.5	<2		2893.0 → 2566.5	13/2 ⁺ → 11/2 ⁺
328.9	4.9(15)	0.89(45)	8866.8 → 8537.9	(33/2 ⁻) → (31/2 ⁻)
343.8	94.6(59)	0.86(11)	5264.1 → 4920.3	21/2 ⁺ → 19/2 ⁺
369.2	2.3(5)		8583.0 → 8213.8	(31/2 ⁻) → (29/2 ⁻)
379.0	3.0(8)	0.68(30)	8213.8 → 7834.8	(29/2 ⁻) → 27/2 ⁽⁺⁾
389.0	13.8(10)	0.91(15)	4838.8 → 4449.8	19/2 ⁻ → 17/2 ⁻
396.6	7.5(24)	1.12(32)	7590.4 → 7193.8	(25/2 ⁺) → (23/2 ⁺)
403.0	33.2(81)	0.75(11)	7834.8 → 7431.8	27/2 ⁽⁺⁾ → 25/2 ⁽⁺⁾
420.0	2.2(8)		8537.9 → 8117.9	(31/2 ⁻) → (29/2 ⁻)
425.3	2.7(6)		5264.1 → 4838.8	21/2 ⁺ → 19/2 ⁻
429.3	28.1(21)	0.74(11)	8264.1 → 7834.8	29/2 ⁽⁺⁾ → 27/2 ⁽⁺⁾
432.3	3.0(6)	0.86(39)	9015.3 → 8583.0	(33/2 ⁻) → (31/2 ⁻)
450.5	<2		3343.5 → 2893.0	13/2 ⁻ → 13/2 ⁺
456.1	18.7(21)	0.74(11)	8720.2 → 8264.1	31/2 ⁽⁺⁾ → 29/2 ⁽⁺⁾
465.1	<2		8583.0 → 8117.9	(31/2 ⁻) → (29/2 ⁻)
470.5	94.9(60)	0.83(19)	4920.3 → 4449.8	19/2 ⁺ → 17/2 ⁻
470.7	28.7(33)	0.54(12)	5309.5 → 4838.8	21/2 ⁻ → 19/2 ⁻
477.8	<2		9903.0 → 9425.2	→ (33/2 ⁺)
478.8	8.7(35)	0.68(31)	10688.6 → 10209.8 _z	(39/2 ⁻) → (37/2 ⁻)
482.0	<2		10385.0 → 9903.0	(35/2 ⁺) →
499.5	5.4(9)	1.14(27)	8089.9 → 7590.4	(27/2 ⁺) → (25/2 ⁺)
509.5	5.4(12)		7184.1 → 6674.6	(25/2 ⁺) → (23/2 ⁺)
571.0	<2		4825.3 → 4254.3	17/2 ⁺ → (15/2 ⁺)
572.5	~8	0.62(27)	9439.3 → 8866.8	(35/2 ⁻) → (33/2 ⁻)
572.8	~4	0.86(24)	11547.2 → 10974.4	(37/2 ⁺) → (35/2 ⁺)
615.2	<2		5879.3 → 5264.1	(19/2 ⁺) → 21/2 ⁺
650.7	15.1(43)	0.78(13)	7834.8 → 7184.1	27/2 ⁽⁺⁾ → (25/2 ⁺)
693.0	28.2(28)	0.77(12)	4825.3 → 4132.3	17/2 ⁺ → 15/2 ⁻
705.0	12.8(19)	0.74(24)	9425.2 → 8720.2	(33/2 ⁺) → 31/2 ⁽⁺⁾
706.5	22.6(23)	1.00(16)	4838.8 → 4132.3	19/2 ⁻ → 15/2 ⁻
757.2	8.0(8)	0.89(31)	7431.8 → 6674.6	25/2 ⁽⁺⁾ → (23/2 ⁺)
770.5	6.5(19)	0.57(25)	10209.8 → 9439.3	(37/2 ⁻) → (35/2 ⁻)
777.0	100.0(62)	0.74(10)	3343.5 → 2566.5	13/2 ⁻ → 11/2 ⁺
788.8	14.8(15)	0.84(18)	4132.3 → 3343.5	15/2 ⁻ → 13/2 ⁻
859.7	<2		5309.5 → 4449.8	21/2 ⁻ → 17/2 ⁻
880.2	6.7(24)	0.60(29)	8117.9 → 7237.7	(29/2 ⁻) → (27/2 ⁻)
909.1			909.1 → 0.0	9/2 ⁺ → 1/2 ⁻
915.8	6.4(15)	0.91(26)	7590.4 → 6674.6	(25/2 ⁺) → (23/2 ⁺)
935.2	47.9(33)	0.67(16)	6199.3 → 5264.1	23/2 ⁺ → 21/2 ⁺
959.8	5.4(11)	0.62(12)	10385.0 → 9425.2	(35/2 ⁺) → (33/2 ⁺)
984.8	3.8(15)		7184.1 → 6199.3	(25/2 ⁺) → 23/2 ⁺
994.5	8.0(12)	0.69(13)	7193.8 → 6199.3	(23/2 ⁺) → 23/2 ⁺
1106.3	71.8(51)	1.20(21)	4449.8 → 3343.5	17/2 ⁻ → 13/2 ⁻
1232.5	28.8(21)	0.72(11)	7431.8 → 6199.3	25/2 ⁽⁺⁾ → 23/2 ⁺
1239.3	60.1(44)	0.64(11)	4132.3 → 2893.0	15/2 ⁻ → 13/2 ⁻
1361.3	<2		4254.3 → 2893.0	(15/2 ⁺) → 13/2 ⁺

TABLE I. (*Continued.*)

E_γ (keV)	I_γ	R_{ADO}	$E_i \rightarrow E_f$ (keV)	$I_i^\pi \rightarrow I_f^\pi$
1365.1	2.7(6)		6674.6 → 5309.5	(23/2 ⁺) → 21/2 ⁻
1410.5	15.7(12)	0.79(20)	6674.6 → 5264.1	(23/2 ⁺) → 21/2 ⁺
1549.2	4.6(11)	0.58(17)	10974.4 → 9425.2	(35/2 ⁺) → (33/2 ⁺)
1657.4	98.1(71)	0.78(13)	2566.5 → 909.1	11/2 ⁺ → 9/2 ⁺
1754.3	5.4(11)		6674.6 → 4920.3	(23/2 ⁺) → 19/2 ⁺
1884.3	<2		7193.8 → 5309.5	(23/2 ⁺) → 21/2 ⁻
1920.0	6.6(18)		7184.1 → 5264.1	(25/2 ⁺) → 21/2 ⁺
1929.7	<2		7193.8 → 5264.1	(23/2 ⁺) → 21/2 ⁺
1932.3	<2		4825.3 → 2893.0	17/2 ⁺ → 13/2 ⁺
1983.9	~90		2893.0 → 909.1	13/2 ⁺ → 9/2 ⁺
1995.6	~4		7259.7 → 5264.1	(23/2 ⁺) → 21/2 ⁺

analysis of present data, the 915.8 keV transition is coincident with the transitions above the $I^\pi = 27/2^+$ level at 7834.8 keV and below the $I^\pi = 21/2^+$ level at 5264.1 keV, but not coincident with the 403.0, 935.2, and 1232.5 keV transitions. Furthermore, based on the coincidence with the 244.4 and 1410.5 keV transitions, the 915.8 keV transition is placed between the 7590.4 and 6674.6 keV levels. The evidence for the new position of the 915.5 keV transition is shown in Figs. 2(a), 2(b), and 2(c). For the negative parity states, two new sequences have been established on the $I^\pi = (27/2^-)$ state at 7237.7 keV and $I^\pi = (29/2^-)$ state at 8213.8 keV. The yrast sequence consists of a cascade of six transitions of energy 880.2, 420.0, 328.9, 572.5, 770.5, and 478.8 keV. In the nonyrast sequence, there is a cascade of two dipole transitions of energy 369.2 and 432.3 keV. The placements of the two sequences are further confirmed by the observation of three linking transitions (283.8, 324.1, and 465.1 keV). The most transitions in two negative sequences can be clearly seen in the Figs. 2(c) and 2(d) gated by the 403.0 and 880.2+328.9 keV transitions. In addition, we also identified four new linking transitions between the positive and negative parity states.

IV. DISCUSSION

Excited states of ^{89}Y have been investigated in the framework of shell model [13–16]. The calculations in Refs. [13,15,16] were performed in the $Z = 28$ –50 model space, i.e., only the proton excitations were considered. Their calculations showed a large difference between the calculated values and experimental data at the high-spin states region, which indicated that cross-shell neutron excitations cannot be ruled out to reproduce the high-spin level structures of ^{89}Y [13,15,16]. So far, the calculations including neutron-core excitations were only carried out in the work of Reif *et al.* [14]. It suggested significant admixtures of the neutron $1g_{9/2}^{-1}2d_{5/2}$ excitations across the $N = 50$ shell for the positive parity states above 4.5 MeV and negative parity states above 7.2 MeV [14]. However, no negative parity states corresponding to this prediction were experimentally observed.

In the present work, the level scheme of ^{89}Y has been extended up to higher spin and excitation energy. In particular, two new negative parity sequences are constructed. To better

reproduce the expanding level scheme of ^{89}Y , we have performed the shell model calculations using the OXBASH [26] code within a larger model space containing the neutron-core excitations across the closed $N = 50$ shell. The model space utilized in the calculations includes four proton orbits ($1f_{5/2}$, $2p_{3/2}$, $2p_{1/2}$, and $1g_{9/2}$) and six neutron orbits ($2p_{1/2}$, $1g_{9/2}$, $1g_{7/2}$, $2d_{5/2}$, $2d_{3/2}$, and $3s_{1/2}$) relative to an inert ^{66}Ni ($Z = 28$, $N = 38$) core. The adopted two-body matrix elements are code named GWBXG.

We have performed two sets of shell model calculations SM-I and SM-II, one (SM-II) allowing neutron excitations across the $N = 50$ shell and the other (SM-I) not. For SM-I, the protons are distributed over the $1f_{5/2}$, $2p_{3/2}$, $2p_{1/2}$, and $1g_{9/2}$ orbits without any truncation. Simultaneously, the neutron shells ($2p_{1/2}$, $1g_{9/2}$) are kept fully occupied, i.e., only the proton excitations are taken into consideration. A single $1g_{9/2}$ neutron across the $N = 50$ shell closure into the $2d_{5/2}$ orbit ($1g_{9/2}^{-1}2d_{5/2}$) is included in SM-II, which leads to a considerable expansion of the configuration space. To make the shell model calculation within SM-II feasible, dimensional restrictions are defined in such a way that at least four protons are constrained on the $1f_{5/2}$ orbit and three protons are constrained on the $2p_{3/2}$ orbit, the other four protons are distributed over the $1f_{5/2}$, $2p_{3/2}$, $2p_{1/2}$, and $1g_{9/2}$ orbits. This means that at most four protons can be lifted to the $1g_{9/2}$ orbit.

Comparisons of the experimental excitation energies for the positive and negative parity states of ^{89}Y with the predictions of shell model calculations are shown in Figs. 3 and 4, respectively. The dominant wave functions of the positive and negative parity states within the SM-II configuration space are listed in Tables II and III, respectively. As shown in Fig. 3, the shell model calculations within the SM-I and SM-II configuration spaces are both in good agreement with the low-lying levels ($9/2^+$ to $15/2^+$) of ^{89}Y . The small differences between the two sets of calculations for the low-lying levels indicate that the proton model space truncation in SM-II is reasonable to interpret the low-lying level structures of ^{89}Y . However, for the high-spin states, there is an obvious divergence between the calculated values of SM-I and experimental data. The calculated results in SM-II can well reproduce the experimental observations, which indicates that the neutron-core excitations must be taken into consideration to interpret the positive parity high-spin states

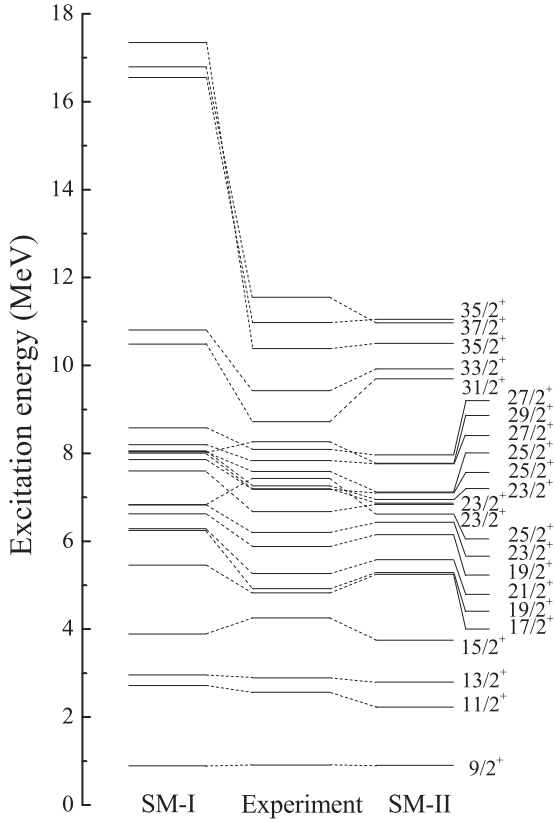


FIG. 3. Comparison of the positive parity states of ^{89}Y with the SM-I and SM-II results performed using the code OXBASH and GWBXG interaction.

in ^{89}Y . In Table II, the $9/2^+$ state comes from one valance proton occupying the $\pi 1g_{9/2}$ orbit, and the main configuration of the $11/2^+$ to $15/2^+$ states is $\pi(1f_{5/2}2p_{3/2})^92p_{1/2}1g_{9/2}$. The configurations of neutron-core excitations appear at the positive parity states with $I^\pi \geq 17/2^+$. The energy where the neutron-core excitations begin to occur is 4825.3 keV. At this energy it is energetically more favorable for ^{89}Y to increase angular momentum by breaking the closed neutron-core than by exciting more protons to the $1g_{9/2}$ orbit. It should be noted, at energies of 6.6–8.3 MeV, the $23/2_1^+$, $25/2_1^+$, $27/2_1^+$, and $29/2_1^+$ states are dominated by the $\pi(1f_{5/2}2p_{3/2})^81g_{9/2}^3$ configuration, which are different with the neighboring $25/2_2^+$, $27/2_1^+$, and $29/2_2^+$ states with the $\pi(1f_{5/2}2p_{3/2})^92p_{1/2}1g_{9/2} \otimes \nu 1g_{9/2}^{-1}2d_{5/2}$ configuration. This indicates a strong competition between the pure proton excitations including the $\pi 1g_{9/2}^3$ component and neutron-core excitations $1g_{9/2}^{-1}2d_{5/2}$ at this energy range in ^{89}Y . Similar behavior is also observed in ^{91}Nb [10] and ^{93}Tc [12]. Above this energy range, the $\pi 1g_{9/2}^3$ component coupled to the $\nu 1g_{9/2}^{-1}2d_{5/2}$ core excitations become energetically more favorable.

For the negative parity states shown in Fig. 4, the shell model calculations within SM-I and SM-II are both in reasonable agreement with the experimental results from the ground state to the $21/2^-$ state. For the states with $I^\pi > 21/2^-$, the SM-II calculation could well reproduce the experimental

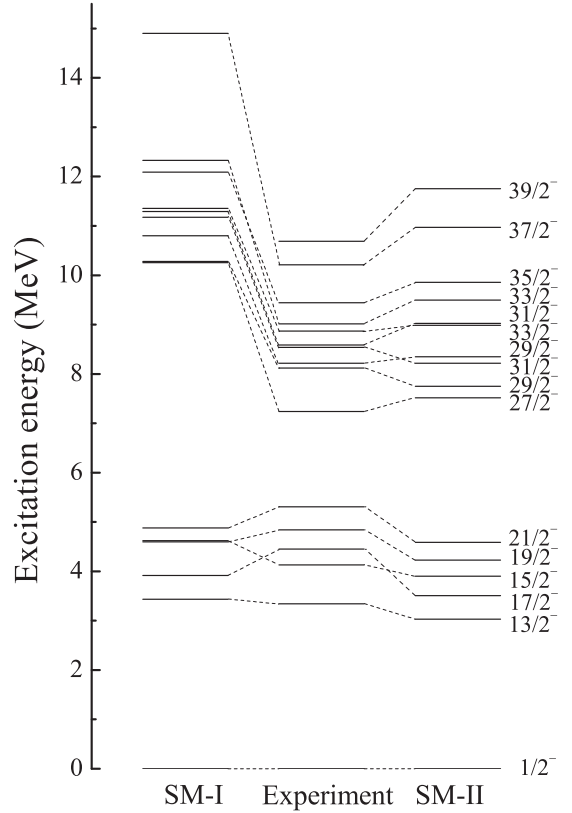


FIG. 4. Similar to Fig. 3 but for the negative parity states.

data, while the SM-I calculation predicts much higher values (about 3 MeV) than the experimental levels. As shown in Table III, the ground state comes from one valance proton occupying the $\pi 1p_{1/2}$ orbit. The main configuration of the $13/2^-$ to $21/2^-$ states is $\pi(1f_{5/2}2p_{3/2})^91g_{9/2}^2$. The breaking of the neutron-core appears from the $I^\pi = 27/2^-$ state. All of the newly observed negative parity levels in the present work come from the neutron-core excitations. It is worth noting that it is the first observation of negative parity states related to neutron-core excitations in ^{89}Y .

Based on the above discussion, the inclusion of a single $1g_{9/2}$ neutron across the $N = 50$ shell closure into the $2d_{5/2}$ orbit is very important for a more complete description of the observed level structures of ^{89}Y . Also, there exists a strong competition between the pure proton and neutron excitations in ^{89}Y at the energy range from 6.6 to 8.3 MeV.

V. NEUTRON-CORE EXCITATIONS IN THE $N = 50$ ISOTONES

The breaking of the neutron-core has been systematically observed in the $N = 50$ isotones [8–13,27,28]. To understand the systematic features of neutron-core excitations, the plot of excitation energies as a function of angular momentum of the states from the neutron excitations in the $N = 50$ isotones [8–13,27,28] is presented in Fig. 5. From Fig. 5, the systematics of the states from the neutron-core excitations in odd- A isotones are very similar with the those in even-even isotones, which indicate that the additional valance proton

TABLE II. The strong components of the wave functions within the SM-II configuration space and their partitions for positive parity states in ^{89}Y .

J^π	Proton				Neutron			Partitions		
	(\hbar)	$1f_{5/2}$	$2p_{3/2}$	$2p_{1/2}$	$1g_{9/2}$	$2p_{1/2}$	$1g_{9/2}$	$1g_{7/2}$	$2d_{5/2}$	%
$9/2^+$	6	4	0	1	2	10	0	0	71.63	
$11/2^+$	6	3	1	1	2	10	0	0	80.09	
$13/2^+$	6	3	1	1	2	10	0	0	68.94	
$15/2^+$	5	4	1	1	2	10	0	0	73.10	
	5	3	2	1	2	10	0	0	16.73	
$17/2^+$	6	4	0	1	2	9	0	1	57.82	
	4	4	2	1	2	9	0	1	17.38	
$19/2^+$	6	4	0	1	2	9	0	1	59.12	
	4	4	2	1	2	9	0	1	16.84	
$19/2_2^+$	6	4	0	1	2	9	0	1	53.13	
	6	3	1	1	2	9	0	1	19.57	
$21/2^+$	6	4	0	1	2	9	0	1	59.87	
	4	4	2	1	2	9	0	1	16.02	
$23/2^+$	6	4	0	1	2	9	0	1	37.75	
	6	3	1	1	2	9	0	1	23.70	
	5	4	1	1	2	9	0	1	18.87	
$23/2_2^+$	5	3	0	3	2	10	0	0	42.62	
	4	4	0	3	2	10	0	0	40.19	
$23/2_3^+$	5	4	1	1	2	9	0	1	48.94	
	6	3	1	1	2	9	0	1	32.62	
$23/2_4^+$	6	3	1	1	2	9	0	1	33.29	
	5	4	1	1	2	9	0	1	27.00	
	6	4	0	1	2	9	0	1	16.05	
$25/2^+$	4	4	0	3	2	10	0	0	69.88	
	4	3	1	3	2	10	0	0	20.90	
$25/2_2^+$	5	4	1	1	2	9	0	1	47.91	
	6	3	1	1	2	9	0	1	25.43	
	5	3	2	1	2	9	0	1	18.46	
$25/2_3^+$	6	3	1	1	2	9	0	1	46.85	
	5	4	1	1	2	9	0	1	36.51	
$27/2^+$	5	4	1	1	2	9	0	1	79.25	
	5	3	2	1	2	9	0	1	15.72	
$27/2_2^+$	4	4	0	3	2	10	0	0	71.82	
	4	3	1	3	2	10	0	0	21.07	
$29/2^+$	4	4	0	3	2	10	0	0	71.23	
	4	3	1	3	2	10	0	0	22.43	
$29/2_2^+$	5	4	1	1	2	9	0	1	48.80	
	5	3	2	1	2	9	0	1	38.66	
$31/2^+$	4	4	0	3	2	9	0	1	74.74	
	4	3	1	3	2	9	0	1	22.72	
$31/2_2^+$	4	4	0	3	2	9	0	1	74.08	
	4	3	1	3	2	9	0	1	15.63	
$33/2^+$	4	4	0	3	2	9	0	1	73.69	
	4	3	1	3	2	9	0	1	22.39	
$33/2_2^+$	4	4	0	3	2	9	0	1	75.94	
	4	3	1	3	2	9	0	1	19.95	
$35/2^+$	4	4	0	3	2	9	0	1	72.94	
	4	3	1	3	2	9	0	1	24.01	
$37/2^+$	4	4	0	3	2	9	0	1	71.18	
	4	3	1	3	2	9	0	1	23.66	

TABLE III. Similar to Table II but for the negative parity states.

J^π	Proton				Neutron				Partitions	
	(\hbar)	$1f_{5/2}$	$2p_{3/2}$	$2p_{1/2}$	$1g_{9/2}$	$2p_{1/2}$	$1g_{9/2}$	$1g_{7/2}$	$2d_{5/2}$	%
$1/2^-$	6	4	1	0	2	2	10	0	0	89.08
$13/2^-$	6	3	0	2	2	10	0	0	0	49.80
	5	4	0	2	2	10	0	0	0	28.22
$15/2^-$	6	3	0	2	2	10	0	0	0	32.06
	5	3	1	2	2	10	0	0	0	19.26
	5	4	0	2	2	10	0	0	0	15.72
$17/2^-$	5	4	0	2	2	10	0	0	0	61.41
$19/2^-$	5	4	0	2	2	10	0	0	0	67.96
$21/2^-$	5	4	0	2	2	10	0	0	0	58.11
	4	4	1	2	2	10	0	0	0	20.02
$27/2^-$	5	4	0	2	2	9	0	1	0	61.67
	5	3	1	2	2	9	0	1	0	20.33
$29/2^-$	5	4	0	2	2	9	0	1	0	65.87
	5	3	1	2	2	9	0	1	0	19.64
$29/2_2^-$	4	4	1	2	2	9	0	1	0	31.00
	5	3	1	2	2	9	0	1	0	24.78
$31/2^-$	5	4	0	2	2	9	0	1	0	65.58
	5	3	1	2	2	9	0	1	0	17.42
$31/2_2^-$	5	3	1	2	2	9	0	1	0	38.62
	4	4	1	2	2	9	0	1	0	36.54
	5	4	0	2	2	9	0	1	0	16.19
$33/2^-$	5	4	0	2	2	9	0	1	0	54.64
	4	4	1	2	2	9	0	1	0	22.88
	5	3	1	2	2	9	0	1	0	17.27
$33/2_2^-$	5	3	1	2	2	9	0	1	0	80.60
$35/2^-$	5	4	0	2	2	9	0	1	0	51.49
	4	4	1	2	2	9	0	1	0	29.30
$37/2^-$	5	3	1	2	2	9	0	1	0	65.94
	4	4	1	2	2	9	0	1	0	30.00
$39/2^-$	5	3	1	2	2	9	0	1	0	54.76
	4	4	1	2	2	9	0	1	0	39.28

do not evidently influence the neutron-core excitations. For positive parity, the levels dominated by the neutron-core excitations are observed above 4 MeV for the $N = 50$ isotones. This implies that the required energy for exciting one neutron across the $N = 50$ shell gap is at least 4 MeV. On the other hand, the negative parity states from the neutron-core excitations appear at the states with $E \geq 6$ MeV, which is about 2 MeV higher than those of the positive parity states. The reason is that the negative parity states need to break a pair of protons and excite a proton to the $1g_{9/2}$ orbit relative to the positive parity states. The energy separation of ~ 2 MeV is consistent with the energy separation between the $9/2^+$ state with $\pi 1f_{5/2}^6 2p_{3/2}^4 1g_{9/2}$ configuration and the $13/2^-$ state with $\pi 1f_{5/2}^6 2p_{3/2}^3 1g_{9/2}^2$ configuration in ^{89}Y . Thus, the positive parity states from neutron-core excitations are generally easier to observe than the corresponding negative parity states.

VI. CONCLUSIONS

High-spin states of the semimagic nucleus ^{89}Y have been investigated via the $^{82}\text{Se}(^{11}\text{B}, 4n)$ reaction at beam energies of

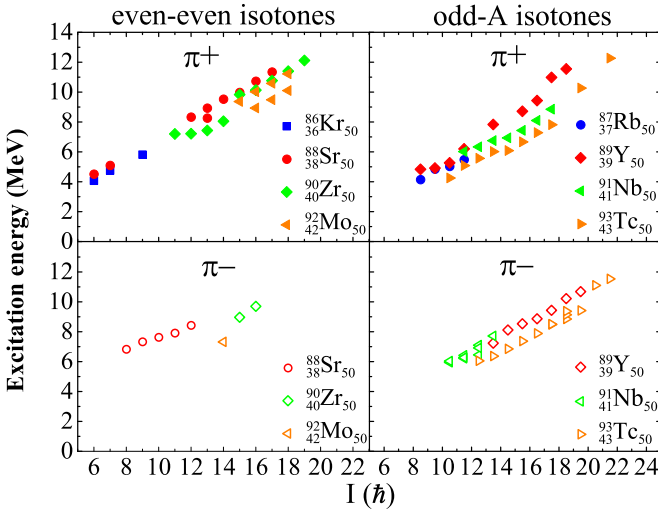


FIG. 5. Excitation energies as a function of angular momentum for the states in the $N = 50$ even-even isotones (left) and odd- A isotones (right) coming from neutron-core excitations across the $N = 50$ gap. The data are from Refs. [8–13,27,28] and the present work. Open and filled symbols denote the positive and negative parity states, respectively.

48 and 52 MeV. A total of 13 new levels and 24 new transitions have been assigned to ^{89}Y . The level scheme has been extended

up to higher spin and excitation energy. Thereinto, two new negative parity sequences have been constructed. Large-basis shell model calculations have been performed to interpret the experimentally observed level structures, which indicates that the neutron-core excitations are essential to reproduce high-spin level structures of ^{89}Y . A competition between the pure proton excitations including the $\pi 1g_{9/2}^3$ component and neutron-core excitations $\nu 1g_{9/2}^{-1}2d_{5/2}$ is suggested in ^{89}Y in the energy range from 6.6 to 8.3 MeV. The systematic features of neutron-core excitations in the $N = 50$ isotones are investigated. It is found that the positive and negative parity states from the neutron-core excitations appear at $E > 4$ and 6 MeV, respectively.

ACKNOWLEDGMENTS

This work is partly supported by the Natural Science Foundation (Grants No. 11545011, No. 11175108, No. 11405096, No. 11461141001, and No. U1432119), the Shandong Natural Science Foundation (Grant No. ZR2014AQ012), and the Young Scholars Program of Shandong University, Weihai (Grant No. 2015WHWLJH01) of China. The computations were carried out on an HP Proliant DL785G6 server hosted by the Institute of Space Science of Shandong University.

- [1] C. Plettner, I. Ragnarsson, H. Schnare, R. Schwengner, L. Käubler, F. Dönau, A. Algara, G. de Angelis, D. R. Napoli, A. Gadea, J. Eberth, T. Steinhardt, O. Thelen, M. Hausmann, A. Müller, A. Jungclaus, K. P. Lieb, D. G. Jenkins, R. Wadsworth, and A. N. Wilson, *Phys. Rev. Lett.* **85**, 2454 (2000).
- [2] J. Ljungvall, A. Görgen, M. Girod, J.-P. Delaroche, A. Dewald, C. Dossat, E. Farnea, W. Korten, B. Melon, R. Menegazzo, A. Obertelli, R. Orlandi, P. Petkov, T. Pissulla, S. Siem, R. P. Singh, J. Srebrny, Ch. Theisen, C. A. Ur, J. J. Valiente-Dobón, K. O. Zell, and M. Zielińska, *Phys. Rev. Lett.* **100**, 102502 (2008).
- [3] R. Wadsworth, I. Ragnarsson, B. G. Carlsson, Hai-Liang Ma, P. J. Davies, C. Andreoiu, R. A. E. Austin, M. P. Carpenter, D. Dashdorj, S. J. Freeman, P. E. Garrett, J. Greene, A. Görgen, D. G. Jenkins, F. Johnston-Theasby, P. Joshi, A. O. Macchiavelli, F. Moore, G. Mukherjee, W. Reviol, D. G. Sarantites, D. Seweryniak, C. E. Svensson, and J. J. Valiente-Dobón, *Phys. Lett. B* **701**, 306 (2011).
- [4] H. Schnare, R. Schwengner, S. Frauendorf, F. Dönau, L. Käubler, H. Prade, A. Jungclaus, K. P. Lieb, C. Lingk, S. Skoda, J. Eberth, G. de Angelis, A. Gadea, E. Farnea, D. R. Napoli, C. A. Ur, and G. Lo Bianco, *Phys. Rev. Lett.* **82**, 4408 (1999).
- [5] R. Schwengner, G. Rainovski, H. Schnare, A. Wagner, F. Dönau, A. Jungclaus, M. Hausmann, O. Iordanov, K. P. Lieb, D. R. Napoli, G. de Angelis, M. Axiotis, N. Marginean, F. Brandolini, and C. Rossi Alvarez, *Phys. Rev. C* **66**, 024310 (2002).
- [6] S. Y. Wang, B. Qi, L. Liu, S. Q. Zhang, H. Hua, X. Q. Li, Y. Y. Chen, L. H. Zhu, J. Meng, S. M. Wyngaardt, P. Papka, T. T. Ibrahim, R. A. Bark, P. Datta, E. A. Lawrie, J. J. Lawrie, S. N. T. Majola, P. L. Masiteng, S. M. Mullins, J. Gál, G. Kalinka, J. Molnár, B. M. Nyakó, J. Timár, K. Juhász, and R. Schwengner, *Phys. Lett. B* **703**, 40 (2011).
- [7] C. Liu, S. Y. Wang, R. A. Bark, S. Q. Zhang, J. Meng, B. Qi, P. Jones, S. M. Wyngaardt, J. Zhao, C. Xu, S.-G. Zhou, S. Wang, D. P. Sun, L. Liu, Z. Q. Li, N. B. Zhang, H. Jia, X. Q. Li, H. Hua, Q. B. Chen, Z. G. Xiao, H. J. Li, L. H. Zhu, T. D. Bucher, T. Dinoko, J. Easton, K. Juhász, A. Kamblawe, E. Khaleel, N. Khumalo, E. A. Lawrie, J. J. Lawrie, S. N. T. Majola, S. M. Mullins, S. Murray, J. Ndayishimye, D. Negi, S. P. Noncolela, S. S. Ntshangase, B. M. Nyakó, J. N. Orce, P. Papka, J. F. Sharpey-Schafer, O. Shirinda, P. Sithole, M. A. Stankiewicz, and M. Wiedeking, *Phys. Rev. Lett.* **116**, 112501 (2016).
- [8] E. A. Stefanova, R. Schwengner, J. Reif, H. Schnare, F. Dönau, M. Wilhelm, A. Fitzler, S. Kasemann, P. von Brentano, and W. Andrejtschef, *Phys. Rev. C* **62**, 054314 (2000).
- [9] E. K. Warburton, J. W. Olness, C. J. Lister, R. W. Zurmühle, and J. A. Becker, *Phys. Rev. C* **31**, 1184 (1985).
- [10] P. W. Luo, X. G. Wu, H. B. Sun, G. S. Li, C. Y. He, Y. Zheng, C. B. Li, S. P. Hu, Y. H. Wu, H. W. Li, J. J. Liu, J. L. Wang, S. H. Yao, and S. A. Edwards, *Phys. Rev. C* **89**, 034318 (2014).
- [11] N. S. Pattabiraman, S. N. Chintalapudi, S. S. Ghugre, B. V. Tirumala Rao, M. L. N. Raju, T. S. Reddy, P. K. Joshi, R. Palit, and H. C. Jain, *Phys. Rev. C* **65**, 044324 (2002).
- [12] M. Hausmann, A. Jungclaus, E. Galindo, K. P. Lieb, O. Yordanov, I. P. Johnstone, R. Schwengner, A. Dewald, A. Fitzler, O. Möller, G. de Angelis, A. Gadea, T. Martinez, D. R. Napoli, and C. Ur, *Phys. Rev. C* **68**, 024309 (2003).
- [13] L. Funke, G. Winter, J. Döring, L. Käubler, H. Prade, R. Schwengner, E. Will, Ch. Protochristov, W. Andrejtschef, L.

- G. Kostova, P. O. Lipas, and R. Wirowski, *Nucl. Phys. A* **541**, 241 (1992).
- [14] J. Reif, G. Winter, R. Schwengner, H. Prade, and L. Käubler, *Nucl. Phys. A* **587**, 449 (1995).
- [15] Michael R. Bunce, Ph.D. thesis, University of Surrey, 2012 (unpublished).
- [16] P. C. Srivastava, Vikas Kumar, and M. J. Ermamatov, *Phys. At. Nucl.* **77**, 1334 (2014).
- [17] M. Davidson, J. Davidson, M. Behar, G. Garcia Bermudez, and M. A. J. Mariscotti, *Nucl. Phys. A* **306**, 113 (1978).
- [18] C. A. Fields and L. E. Samuelson, *Phys. Rev. C* **20**, 2442 (1979).
- [19] E. K. Warburton, J. W. Olness, C. J. Lister, J. A. Becker, and S. D. Bloom, *J. Phys. G* **12**, 1017 (1986).
- [20] T. Batsch, J. Kownacki, Z. Źelazny, M. Guttormsen, T. Ramsøy, and J. Rekstad, *Phys. Scr.* **37**, 843 (1988).
- [21] C. J. Xu, S. Y. Wang, C. Y. Niu, C. Liu, B. Qi, D. P. Sun, L. Liu, P. Zhang, Z. Q. Li, Z. Wang, X. G. Wu, G. S. Li, C. Y. He, Y. Zheng, B. B. Yu, C. B. Li, S. P. Hu, S. H. Yao, X. P. Cao, and J. L. Wang, *Phys. Rev. C* **86**, 027302 (2012).
- [22] M. Piiparinen, A. Ataç, J. Blomqvist, G. B. Hagemann, B. Herskind, R. Julin, S. Juutinen, A. Lampinen, J. Nyberg, G. Sletten, P. Tikkanen, S. Törmänen, A. Virtanen, and R. Wyss, *Nucl. Phys. A* **605**, 191 (1996).
- [23] E. A. Stefanova, R. Schwengner, G. Rainovski, K. D. Schilling, A. Wagner, F. Dönau, E. Galindo, A. Jungclaus, K. P. Lieb, O. Thelen, J. Eberth, D. R. Napoli, C. A. Ur, G. de Angelis, M. Axiotis, A. Gadea, N. Marginean, T. Martinez, Th. Kröll, and T. Kutsarova, *Phys. Rev. C* **63**, 064315 (2001).
- [24] N. Fotiades, J. A. Cizewski, R. Krücken, R. M. Clark, P. Fallon, I. Y. Lee, A. O. Macchiavelli, D. P. McNabb, J. A. Becker, L. A. Bernstein, and W. Younes, *Phys. Rev. C* **71**, 064312 (2005).
- [25] H. Rotter, J. Döring, L. Funke, L. Käubler, H. Prade, R. Schwengner, G. Winter, A. E. Zobov, A. P. Grinberg, I. Kh. Lemberg, A. S. Mishin, L. A. Rassadin, I. N. Chugunov, A. D. Efimov, K. I. Erokhina, V. I. Isakov, L. O. Norlin, and U. Rosengård, *Nucl. Phys. A* **514**, 401 (1990).
- [26] B. A. Brown, A. Etchegoyen, N. S. Godwin, W. D. M. Rae, W. A. Richter, W. E. Ormand, E. K. Warburton, J. S. Winfield, L. Zhao, and C. H. Zimmerman, OXBASH for Windows, MSU-NSCL Report No. 1289, 2004 (unpublished).
- [27] G. Winter, R. Schwengner, J. Reif, H. Prade, L. Funke, R. Wirowski, N. Nicolay, A. Dewald, P. von Brentano, H. Grawe, and R. Schubart, *Phys. Rev. C* **48**, 1010 (1993).
- [28] Y. H. Zhang, Zs. Podolyàk, G. de Angelis, A. Gadea, C. Ur, S. Lunardi, N. Marginean, C. Rusu, R. Schwengner, Th. Kröll, D. R. Napoli, R. Menegazzo, D. Bazzacco, E. Farnea, S. Lenzi, T. Martinez, M. Axiotis, D. Tonev, W. Gelletly, S. Langdown, P. H. Regan, J. J. Valiente Dobon, W. von Oertzen, B. Rubio, B. Quintana, N. Medina, R. Broda, D. Bucurescu, M. Ionescu-Bujor, and A. Iordachescu, *Phys. Rev. C* **70**, 024301 (2004).